Title
Voltage-gated potassium channel opening

Author
Lent, Michelle Anne

Publication Date
2006

Peer reviewed|Thesis/dissertation

Voltage-Gated Potassium Channel Opening: A Study of the Inner Helix 'Hinge' Motif

by

Michelle Anne Lent

THESIS

Submitted in partial satisfaction of the requirements for the degree of

MASTER OF SCIENCE

in

Biophysics

in the

GRADUATE DIVISION

of the

UNIVERSITY OF CALIFORNIA, SAN FRANCISCO

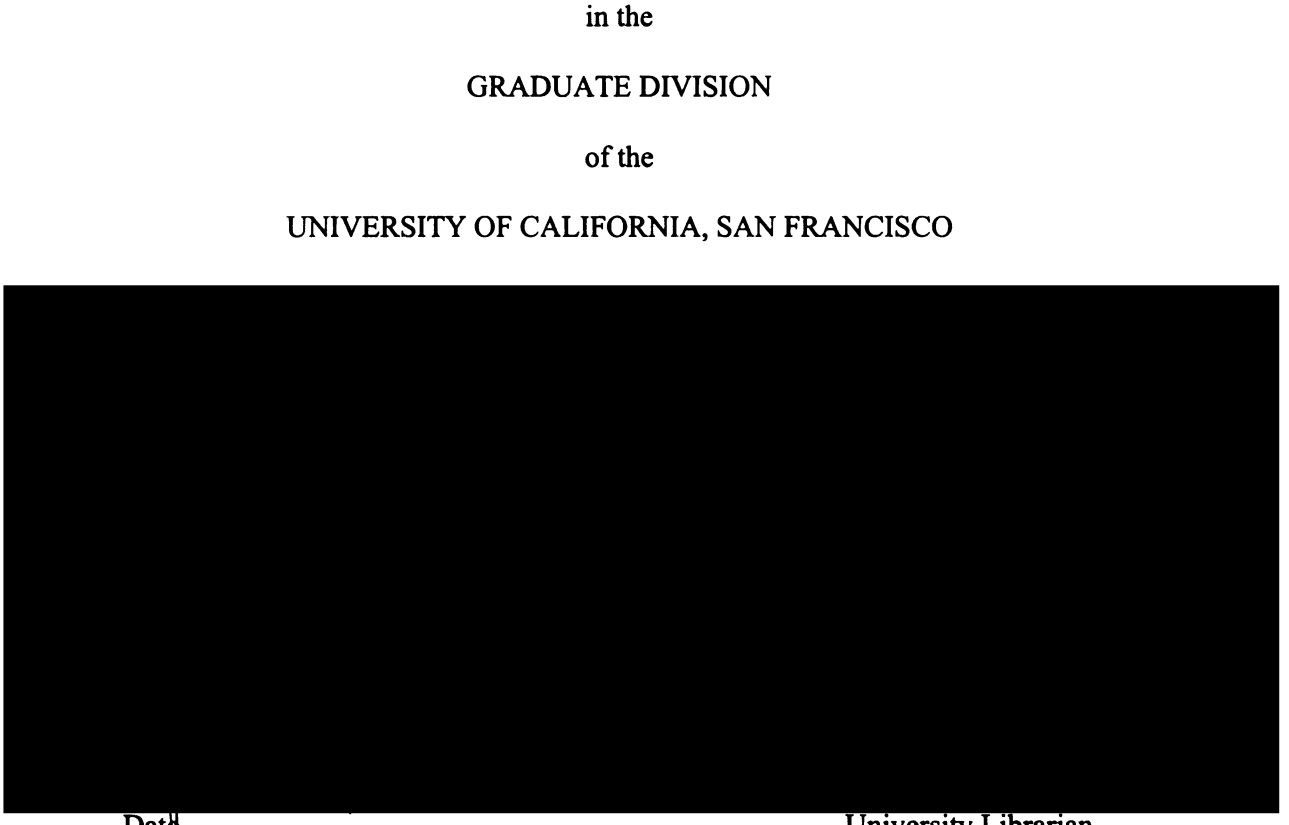

Date University Librarian

Degree Conferred:.....

Acknowledgements

I would like to thank my advisor, Lily Jan, for always being supportive and giving me the freedom to figure out my style and path. Lily Jan and Yuh Nung Jan have created a diverse, lively laboratory environment, and I have been lucky to work with people of such high scientific caliber.

Michael Grabe has not only been my main collaborator, but he has also become a good friend and a mentor. With his incredibly creative and quantitative mind, I am sure he will do wonderfully in his new position as faculty at University of Pittsburgh.

Delphine Bichet and Taihao Jin took on the experimental aspects of my project, creating mutant constructs and performing electrophysiology recordings.

Table of Contents

List of Figures

ABSTRACT

Voltage-gated potassium (Kv) channels control the excitability of neurons and muscles, and their malfunctions have been linked to human diseases including epilepsy, deafness, arrhythmia, episodic ataxia and myokymia (Ashcroft, 2006). Crucial for their functions is the gating mechanism underlying channel opening. Here we report studies suggesting that residues preceding the PVP motif in the pore-lining inner helix S6 are critical for helix bending and channel gating. Specifically, we suggest an expanded Kv gating motif: **A**/S-**L**/M-**P**-**V**/I-**P**. Indeed, mutational effects on channel gating can be accounted for and predicted by the energy landscape generated by constrained simulations of the motion of the S6 segment of Kv1.2.

INTRODUCTION

The potassium ion concentration gradient across the cell membrane allows potassium channels to control membrane potential; increased potassium channel activity tends to hyperpolarize the cell, driving the membrane potential towards the potassium equilibrium potential. The activity of voltage-gated potassium channels, in turn, is controlled by membrane potential, thereby enabling these channels to regulate neuronal excitability – upon the initiation of an action potential Kv channels open and drive the membrane potential back to the resting membrane potential of the cell, thus bringing the action potential to an end. The opening and closing of channels, called gating, is ultimately achieved by mechanically altering the channel structure between states that either permit or obstruct the flow of ions through the channel. Proper channel function

depends critically on this gating process. Defects in channel gating give rise to a number of diseases; for example, both epilepsy and cardiac arrhythmias can stem from Kv channel mutations that alter the gating properties (Lehmann-Horn and Jurkat-Rott, 1999).

Extensive mutagenesis studies and structural analyses have implicated the pore-lining inner helix as a gate that adopts different conformations in open versus closed channels. In the closed state, the pore-lining inner helices of the channel's tetrameric structure form an inverted 'teepee' resulting in a helical bundle at the apex that blocks the ion pathway (Doyle *et al.*, 1998). In the open state, these inner helices appear to splay out, away from the central pore, allowing an unobstructed pathway for ions to move through the channel (Jiang *et al.*, 2002b). It has been suggested that the channel opens like a camera aperture (Jiang *et al.*, 2003a). Comparison of the open-state MthK and the closed-state KcsA channel structures suggests a hinge point at a conserved glycine along the inner helices of these two transmembrane domain (2-TM) channels, which are formed by four subunits each containing two membrane-spanning helices (Jiang *et al.*, 2002b). As for the 6-TM Kv channels (formed by four subunits each with six transmembrane segments), the bacterial KvAP structure appears to have a bend centered on the same conserved glycine (Jiang *et al.*, 2003a). Whereas mutagenesis studies of 2-TM potassium channels have found the conserved 'hinge' glycine of the inner helix to be essential for channel function (Minor *et al.*, 1999; Jin *et al.*, 2002), the inner helix S6 of the 6-TM Kv channels contains a Pro-x-Pro region that is largely conserved across eukaryotic Kv potassium channels and critical for channel gating (Labro *et al.*, 2003; Webster *et al.*, 2004). Both functional studies employing channel blockers and crystallography of Kv1.2

support the notion that the inner helices of open Kv channels are bent at the P-x-P region (del Camino *et al.*, 2000; Long *et al.*, 2005). Moreover, whereas substitution of the S6 prolines by alanine or glycine compromised channel gating (Labro *et al.*, 2003), channel function could be rescued by reintroducing prolines at particular positions above and below the motif region, confirming the importance of prolines (but obscuring the exact role of the P-x-P motif in gating).

Given that no open- and closed-state structures have been determined for any one type of ion channel, how exactly the channel conformation is altered during gating remains an open question. For cyclic nucleotide-gated ion channels, Clayton *et al.* (2004) proposed a gating model based on the crystal structures of liganded and unliganded cyclic nucleotide binding (CNB) domains. In a cyclic nucleotide-gated cation channel, four CNB domains, each linked to an inner helix, form an intracellular ring and, upon ligand binding, cause a conformational change that is transmitted to the channel's inner helices, the 'gate', presumably enlarging the diameter of the area encircled by the inner helices by 7 Å (Clayton *et al.*,2004). For the 2-TM KcsA potassium channel, spin-labeling and electron paramagnetic resonance (EPR) spectroscopy studies suggest that the inner helices both translate outward and rotate counterclockwise relative to the pore (as seen from the extracellular side), increasing the pore diameter and thus opening the channel (Perozo *et al.*, 1999). While certain glycine or proline residues in the inner helix have been found in numerous studies to be critical to channel gating, just how these residues contribute to channel gating are not well understood (Ri *et al.*, 1999; del Camino *et al.*, 2000; Hackos *et al.*, 2002; Jin *et al.*, 2002; Labro *et al.*, 2003; Magidovich and Yifrach, 2004; Seebohm *et al.*, 2006).

It has been well established that both glycine and proline play important roles in allowing α -helices to deviate from their ideal conformations. Gly and Pro residues increase helix flexibility and both are prevalent at kinks in α-helices. Glycine allows helix flexibility and kinking simply because it itself has a large range of movement due to the small size of its side chain (Chou and Fasman, 1974). On the other hand, proline is a fairly rigid residue, given that it has one fixed dihedral angle. However, proline introduces helix flexibility by disrupting hydrogen bonding: the carbonyl oxygen of the i-4 residue cannot form its usual hydrogen bond to the ith residue when that position is occupied by a proline, which results in greater range of movement for the i-4 residue. The residue directly preceding the proline also takes on atypical dihedral angles (Karplus, 1996). This disruption of backbone hydrogen bonding and introduction of unusual dihedral angles often provides the basis for helix kinking.

In this study we investigated the different inner helix conformations from the putative open-state potassium channel crystal structures and discovered an unusual set of dihedral angles of the Kv1.2 S6 segment preceding the bending of this pore-lining inner helix. We then pursued the possibility of a causal relationship between the unusual dihedral angles and the bending of the helix through computational studies. Using molecular dynamics (MD) simulations, we analyzed S6 bending and obtained local elasticity and bending anisotropy information along the helix, and further tracked helix tail movements with respect to the dihedral angles of interest. From these simulations we calculated energetics of transition from the bent S6 conformation of an open channel to the straight S6 conformation of the closed channel. To validate the bent-to-straight transition energies obtained from the MD simulations, we "mutated" Kv1.2 S6 residues

in silico and compared the Ramachandran plots of various amino acids with the dihedral angles of the specific S6 residues. We further computed the bending moduli and energetics of the S6 segment carrying the mutation, and then checked against experimental data, thereby verifying the critical roles of residues preceding the prolines in predisposing helix bending during channel gating.

METHODS

Simulation Systems

The starting structure was the S6 helix (residues 385-418) from the crystal structure of Kv1.2 (pdb code 2A79). The backbone atoms of residues 385-400 were restrained, mimicking the top of S6 being nestled between neighboring S5 and P-loop regions. The helix termini were not modified. The sole lysine residue was protonated, while the histidine residue was not. A chloride ion was added for electroneutrality. Point mutations were made with NAMD Psfgen. For solvated systems, VMD Solvate package was used to add a $0.1 \times 0.1 \times 0.1$ nm water box around the helix, resulting in 16,242 (wild-type), 16,239 (P405A), 16,745 (L404A), 16,739 (L404I), or 16,742 (A403V & A403G) water molecules. All structures were minimized and annealed in NAMD prior to MD.

Simulation Protocol

All simulations were run under NVT conditions using NAMD with a CHARMM force field. PME electrostatics were used with a dielectric of 1.0 and periodic boundary

conditions. A 1.0 nm electrostatics and van der Waals cut-off was employed with a 0.8 nm switch distance and a 1.1 nm pair list distance. The time step was 2 fs, and the neighbor list was updated every 10 steps. The system was maintained around 300 K using Langevin temperature coupling with a damping constant of 10 ps^{-1}. The SHAKE algorithm was used to constrain the length of the bond between an hydrogen and its mother atom.

Each "dihedral-adjusted" simulation contained 20 150 ps steps, each with a different (ϕ, ψ) constraint for the dihedrals of interest. The first 50 ps of each step were for equilibration purposes and only the later 100 ps were recorded, resulting in 2 ns recorded runs. For each case, i.e. wild-type or various mutants, five simulations were compiled for a total of 10 ns. Control simulations with either fixed dihedral constraints or no constraints were 2 ns long and did not require mid-run equilibration steps since there were no constraint changes shifting the underlying energy potential. Each control simulation was run three times for a total runtime of 6 ns per different set-up.

The dihedrals of interest were constrained about particular angle values by a harmonic force with a spring constant of 10 kcal/mol × rad^{-2}. After the simulation, the dihedral restraint energy was removed from the system's energy via the Weighted Histogram Analysis Method (WHAM), as described by Kumar *et al.*, 1992 and 1995. For equilibrium (unrestrained) simulations, the elastic bending moduli were calculated as described by Choe and Sun, 2005. All analysis code was written and run in Matlab™.

RESULTS

Comparing the inner helices of putative open-state channels (Fig.1a) suggests that there are at least two different modes by which potassium channel inner helices can rearrange to allow the channel to open: curving and kinking. In this paper, curving refers to a non-localized hinge angle, i.e. the strain is spread over a number of residues, whereas kinking occurs when the helix hinge angle is highly localized. The KvAP inner helix appears to bend in such a way that the distortion is spread over numerous residues. It was suggested that the KvAP hinge is focused on the glycine that corresponds to the hinge glycine in MthK (Jiang *et al.*, 2003a), but it appears the bend spans between the conserved glycine and a glycine two turns up the helix and the voltage sensors in the KvAP structure are not positioned as expected for an open channel. In contrast, MthK and Kv1.2 both kink at a highly localized hinge point along the inner helix.

To investigate the difference between the various open-state inner helices, we determined the local kink angle and the backbone dihedral angles for each bent helix (Fig. 2). The local kink angle is defined by the angle between local axes for eight residues above and below the origin (see Fig. 1b). The origin is moved down the helix residue by residue to obtain the local kink angles.

An ideal right-handed α-helix has phi (ϕ) and psi (ψ) values of –60° and –45°, respectively. A helical residue is defined as having angles: $\phi = -60° \pm 30°$ and $\psi = -47 \pm 30°$ (Garcia and Sanbonmatsu, 2001). As expected, the largest kink angle in MthK inner helix occurs at Gly^{83}, the hinge residue (Jiang *et al.*, 2002); however, interestingly, the largest dihedral angle distortions away from helical values occur at the residues surrounding Gly^{83}, not at the hinge residue itself (Fig. 2). There is no definitive kink

angle in KvAP, which fits with its non-localized bending. Also, all of the KvAP inner helix dihedral angles remain within normal helical values, which is not surprising since there is no large localized helix distortion. Along the Kv1.2 inner helix the largest kink occurs at the P-V-P region, a region that has a role in gating according to experimental evidence (del Camino *et al.*, 2000; Labro *et al.*, 2003). There is a dramatic distortion in the dihedral angles of the residues directly preceding this P-V-P region. This proximity of angle distortion and helix distortion suggests a potential correlation between the non-helical backbone dihedral angles, phi of Leu^{404} (ϕ^{404}) and psi of Ala^{403} (ψ^{403}), and the largest kink angle at the subsequent Val^{406} flanked by prolines. Perhaps ϕ^{404} and ψ^{403} are control parameters for the helix kinking. If that is the case, one could imagine that adjusting the distorted dihedral angles to helical values would straighten out the helix.

To test if there is a correlation between (ϕ^{404}, ψ^{403}) and helix kinking, MD simulations were run on the Kv1.2 inner helix with the (ϕ^{404}, ψ^{403}) values brought to helical values through stepwise constraints over a multi-step simulation. It appears that an adjustment of the distorted dihedral angles to helical values straightens out the helix (Fig. 3a), in effect closing the channel. For a rigorous study of helix movements between the end states, helix tail movements relative to an ideal straight helix were tracked over a plane perpendicular to the end of an ideal straight helix (Fig. 3b). The plane's origin is defined by where the ideal straight helix would hit the plane. There indeed seems to be a correlation between the (ϕ^{404}, ψ^{403}) values and the movement of the lower portion of the helix (Fig. 3c). However, the appearance of correlation could be attributed to the helix relaxing to a straight conformation on a similar time scale to the angle value changes. To investigate this possibility, we performed control simulations with (ϕ^{404}, ψ^{403}) held at their

initial crystal structure values. If (ϕ^{404}, ψ^{403}) are not correlated with the movement of the lower portion of the helix, the helix should be able to relax to a straight conformation regardless of those particular dihedral values. The control demonstrated that when (ϕ^{404}, ψ^{403}) are held at their crystal structure values the helix cannot straighten (Fig. 3d), strongly suggesting (ϕ^{404}, ψ^{403}) play a major role in directing the helix tail movements. This correlation suggests Ala^{403} and Leu^{404} may be important for gating. Since functionally important residues are generally highly conserved, we asked whether Ala^{403} and Leu^{404} are conserved in channels with the P-V/I-P motif.

Both Ala^{403} and Leu^{404} are highly conserved in channels with the P-V/I-P motif (Fig. 4). Each position has one alternate amino acid: Ser^{403} and Met^{404}. These alternate residues are surprising given that there are other amino acids closer in size and hydrophobicity to the consensus residues, *e.g.* Gly or Val for Ala and Ile for Leu. If size and hydrophobicity are not the most important determinants, what is? The answer lies in the amino acids' Ramachandran plots. We plotted the dihedral angles of Ala^{403} and Leu^{404} from the Kv1.2 crystal structure on their respective Ramachandran plots, as well as on other Ramachandran plots of interest (Fig. 5).

Are the pre-kink residues Ala^{403} and Leu^{404}, which take on values dramatically outside the normal α-helical dihedral range, essential to the helix's ability to kink? There are known mutations at these two positions. Ala^{403}Val abolishes channel expression in Shaker (Yifrach and MacKinnon, 2002) and the corresponding mutation in the KCNQ1 channel, Ala^{341}Val, is implicated in long QT syndrome, a cardiac arrhythmia (Korobi *et al.*, 2003). Leu^{404}Ala reduces Shaker channel function (Yifrach and MacKinnon, 2002) and the corresponding mutation in KCNQ1 reduces channel function as well (Seebohm,

2006). Given that alanine has a smaller sidechain and, consequently less constraint on its conformation, it seems surprising that a leucine to alanine mutation would decrease the helix's ability to bend open. However, comparing the leucine and alanine Ramachandran plots suggests that it is indeed harder for the alanine residue to take on the x-ray structure residue 404 dihedral values (Fig. 5). An alternative explanation is that Leu plays an important role in protein packing for proper channel function, which is possible as it is within 5Å of several residues on a neighboring S6 helix.

Do residues 403-405 play important roles in directing helix tail motions? We looked at the effects of wild-type and mutant residues at these positions on helix bending motions by calculating bending moduli from unconstrained runs. By tracking the relative motion between helix sections, or 'slices', one can determine the stiffness and anisotropy of bending along a helix. We used the helix configurations generated by the MD simulations and calculated probability distributions for the position of a three-residue slice relative to its neighbor triad for several turns surrounding the PVP motif (Fig. 6), with the change between slices IAL and PVP shown in the second row and the preceding (VLT-IAL) and subsequent changes (PVP-VIV) shown in the top and bottom rows, respectively. A single-peak distribution centered on zero reflects a helix that has no intrinsic bend, and thus flexes isotropically, whereas a displaced single-peak distribution implies that helix has a natural tendency to kink in a preferred direction, ω_1 or ω_2, or twist along its axis, ω_3. For instance, each residue in an ideal α-helix corresponds to a 100° (1.75 rad) rotation of the helix and a 1.5 Å translation along its axis. Therefore, we expect ω_3 to be centered on the value $(2\pi - 3 \cdot 1.75)/(3 \cdot 1.5\ \text{Å}) \sim 0.23\ \text{Å}^{-1}$, which is indeed the predominant ω_3 mode seen in our simulations (data not shown). A bimodal

distribution reflects a propensity for the helix to take on two distinct states, such as straight and bent. In general, the flexibility of the helix is proportional to the width of this distribution.

We found that the wild-type (wt) helix has a bimodal ω_1 distribution for the bending between IAL-PVP slices (the second row in Fig. 6b), suggesting that region only bends in specific directions, much like a hinge that can take on two positions. Both peaks are shifted left from the zero point, suggesting the conformations are 'bent' and 'more bent'. The distribution is biased towards the straighter of the two bent conformations. Directly preceding and following this position, the helix takes on a single configuration. The corresponding position in the $P^{405}A$ mutant, IAL-AVP, also exhibits a bimodal ω_1 distribution but with the distribution shifted such that one of the peaks lines up with zero (straight conformation). Also the relative populations of the two states shifted such that the helix seems to spend nearly equal time in the bent and straight conformations. This supports the idea that the Pro to Ala mutation disrupts the inherent bending propensity or 'hinge'. Besides changing the bending conformations, the proline to alanine mutation also increases the general floppiness as seen in the increased distribution width (first and second row in Fig. 6b and 6c). Similarly, mutating Ala^{403} to Gly greatly increases helix flexibility (first row in Fig. 6b). Mutating Leu^{404} to Ala or Ile does not greatly impact the stiffness or directionality of bending compared to wt for either ω_1 or ω_2; however, Ala slightly enhances the separation between peaks at IAL-PVP and Ile reduces the population of the more highly kinked state (second row in Fig. 6b). The torsional distributions about the PVP region presented here are much more complex than those reported for random and polyglycine helices (Choe and Sun 2005), and the emergence of

bimodal distributions suggests that these sequences are inherently bistable which is consistent with the helix's role as a 'gate'.

To resolve the actual directions of helix tail movements, we mapped the energies obtained from angle-adjusted MD simulations as a function of the helix tail position (Fig. 7a). The resulting landscape gives the energy difference between the straightened helix and various bent conformations. We calculated the energy difference between the crystal structure (open-state) conformation and the straightened (closed-state) conformation for the wt and mutant helices. For the wt helix (Fig. 7b), the open-state is 2-3 k_BT higher than the closed-state conformation. Furthermore, there appears to be an energy barrier that functions to constrain or guide the helix motion and prevent over-kinking, i.e. bending past the open-state conformation.

When Pro^{405} is mutated to Alanine (Fig. 7c), the energy difference increases to about 5 k_BT, implying that the helix is twice as hard to bend to the open-state conformation. This increase in bending energetics provides an explanation for why this mutation eliminates channel activity. Besides impacting the energy difference between the open- and closed-state conformations, the Pro to Ala mutation changes the entire energy landscape. The helix is no longer constrained to move between the two conformations, consistent with our analyses of the bend moduli, and it can, in fact, bend much farther way from the pore than the wt helix.

When Ala^{403} is mutated to Gly (Fig. 7d), the energy landscape flattens dramatically. The mutant helix can bend in many more directions without incurring an energetic penalty, consistent with the increased flexibility shown in the bending moduli analysis. It is likely that this mutant channel would open more easily than wt. A lower

energy barrier between the open- and closed-state conformations could also lead to faster channel kinetics.

For the Leu^{404} to Ala mutant (Fig. 7e), the energy of bending to the open-state conformation increases 1-2 k_BT relative to that of the wt channel. Interestingly, the energies obtained from the simulations are consistent with the reported values based on electrophysiological recordings of this mutant channel: $\Delta\Delta E \sim 1.5\ k_BT$ (Yifrach and MacKinnon, 2002) and 3.8 k_BT (Hackos *et al.*, 2002) relative to wt (positive $\Delta\Delta E$ = harder to open). The agreement between the measured energy change and our computations suggest that the mutant residue mainly affects helix bending mechanics, as opposed to packing.

When Leu^{404} is mutated to Ile (Fig. 7f), the mutant helix has an open-state conformational energy similar to that of wt. However, the $L^{404}I$ helix never straightens during the 10 ns of MD simulation runs (unlike wt and all the other mutants!), suggesting that its closed-state conformation would be at much higher energy than that of wt. Perhaps a channel with this mutation would be constitutively open.

DISCUSSION

In this study, we discovered an unusual set of dihedral angles of the Kv1.2 S6 segment directly preceding the PVP kink. Through molecular dynamics simulations we found that these two particular dihedral angles exert control over the S6 helix tail movements. Moreover, bringing these angles from their initial crystal structure values to standard α-helical values straightens the helix, in effect closing the channel (as shown by

overlaying the S6 helix on the rest of the pore domain). We investigated various mutations in this region *in silico* and we obtained energy landscapes for wt and mutant helices moving between the initial kinked (open-state) conformation and a straightened (closed-state) conformation. We are in the process of experimentally investigating the predicted mutations, except for $A^{403}V$, which is non-expressing (Yifrach and Mackinnon, 2002) and $P^{405}A$, which is nonconducting (Hackos *et al.*, 2002). Preliminary data demonstrate that both $A^{403}G$ and $L^{404}I$ mutations result in functional channels. Once we have obtained electrophysiology data on the $A^{403}G$ and $L^{404}I$ mutant channels we can compare the computational data to the experimental results.

This study did not consider the conserved glycine that corresponds to the MthK 'hinge' glycine. While there is experimental evidence supporting the homologous residue (Gly^{398} in Kv1.2) playing a role in channel gating (Magidovich and Yifrach, 2004; Ding *et al.*, 2005), this residue does not correspond to a kink region in the Kv1.2 crystal structure. Of course, a crystallized structure only gives one conformation out of numerous possibilities, and perhaps there exist conformations with bending at both the glycine and the (AL)PVP region.

Future directions

We are collecting electrophysiology data on the $A^{403}G$ and $L^{404}I$ mutant channels using the two-electrode voltage clamp recording technique. Two-electrode voltage clamp recording gives macroscopic ionic and gating currents, from which the energy between open- and closed-state can be calculated, allowing direct comparison with the computed energy. To pursue a more detailed understanding of the mutant channels, we can perform

single channel recording which gives gating kinetics information, such as open probabilities.

If the experiments end up supporting the computational predictions, perhaps there are other mutations that could studied in this manner. This type of computational study takes less time and resources than the corresponding experiment. Accordingly, one could use this analysis to identify potentially interesting mutants rather than experimentally screening by hand.

Another possible computational study would be to apply a force to the end of the crystal structure conformation of the Kv1.2 S6 helix that pulls it to the straightened conformation. Of course, there would be the issue of how and which way to pull on the helix and on what timescale, but, nonetheless, it would be interesting to compare the helix bending energetics obtained by the two different methods.

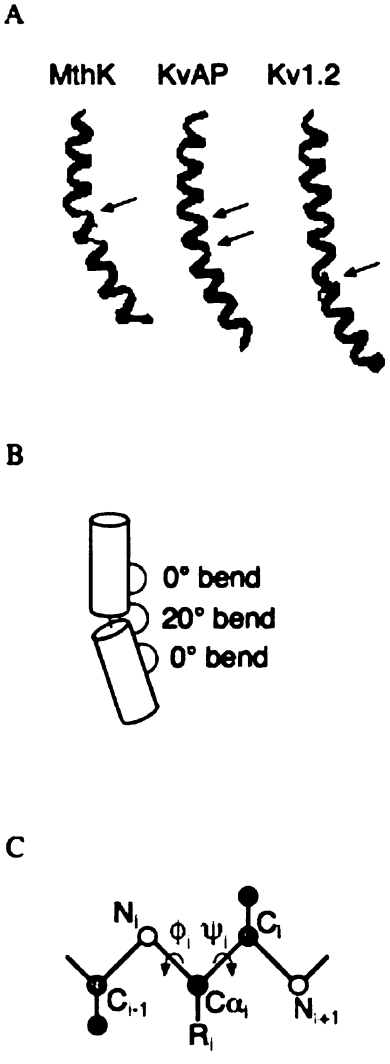

Figure 1: A) Variation in open-state inner helices for three different channel structures: curve versus kink, B) example of local helix angles and C) dihedral angle explanatory diagram. In A), the 'hinge' residues are shown as purple sidechains and marked by arrows.

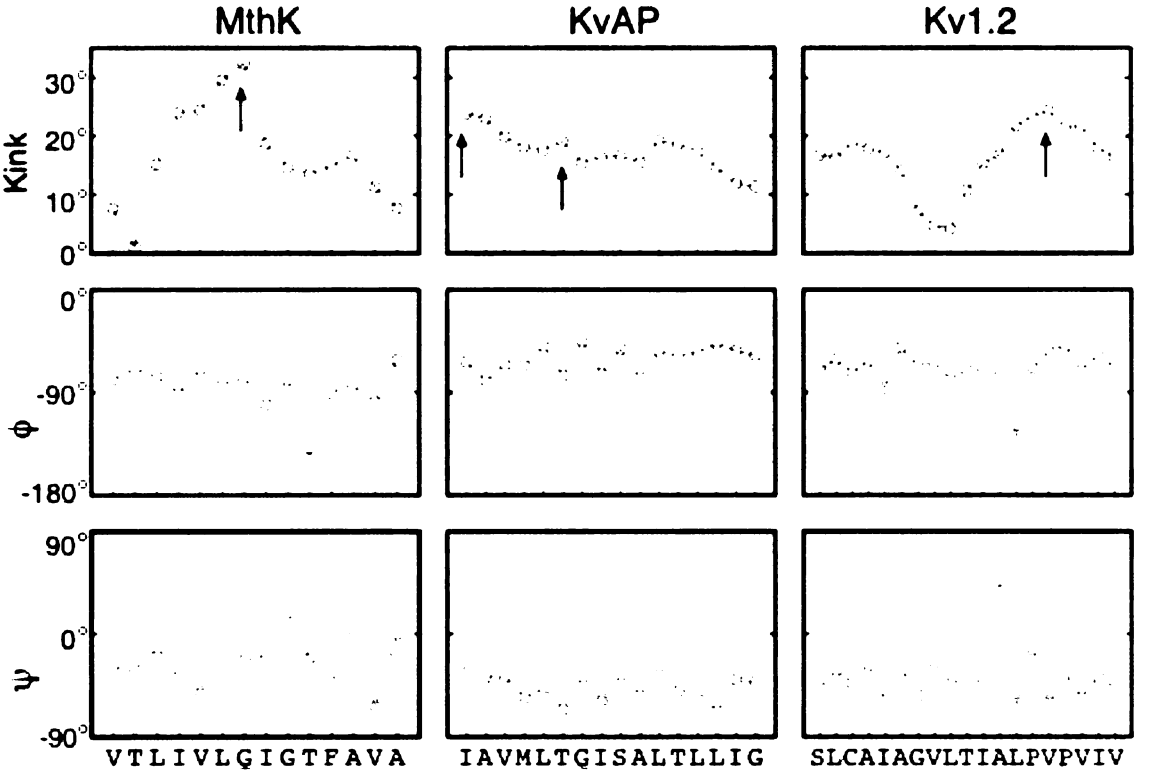

Figure 2: Kink angles and backbone dihedral angles along inner helices of open-state potassium channel crystal structures from Figure 1A. The arrows mark the points of greatest local helix bending, and the corresponding hinge residues are underlined. The cyan and magenta lines mark the edges of the α-helical angle range for phi and psi, respectively.

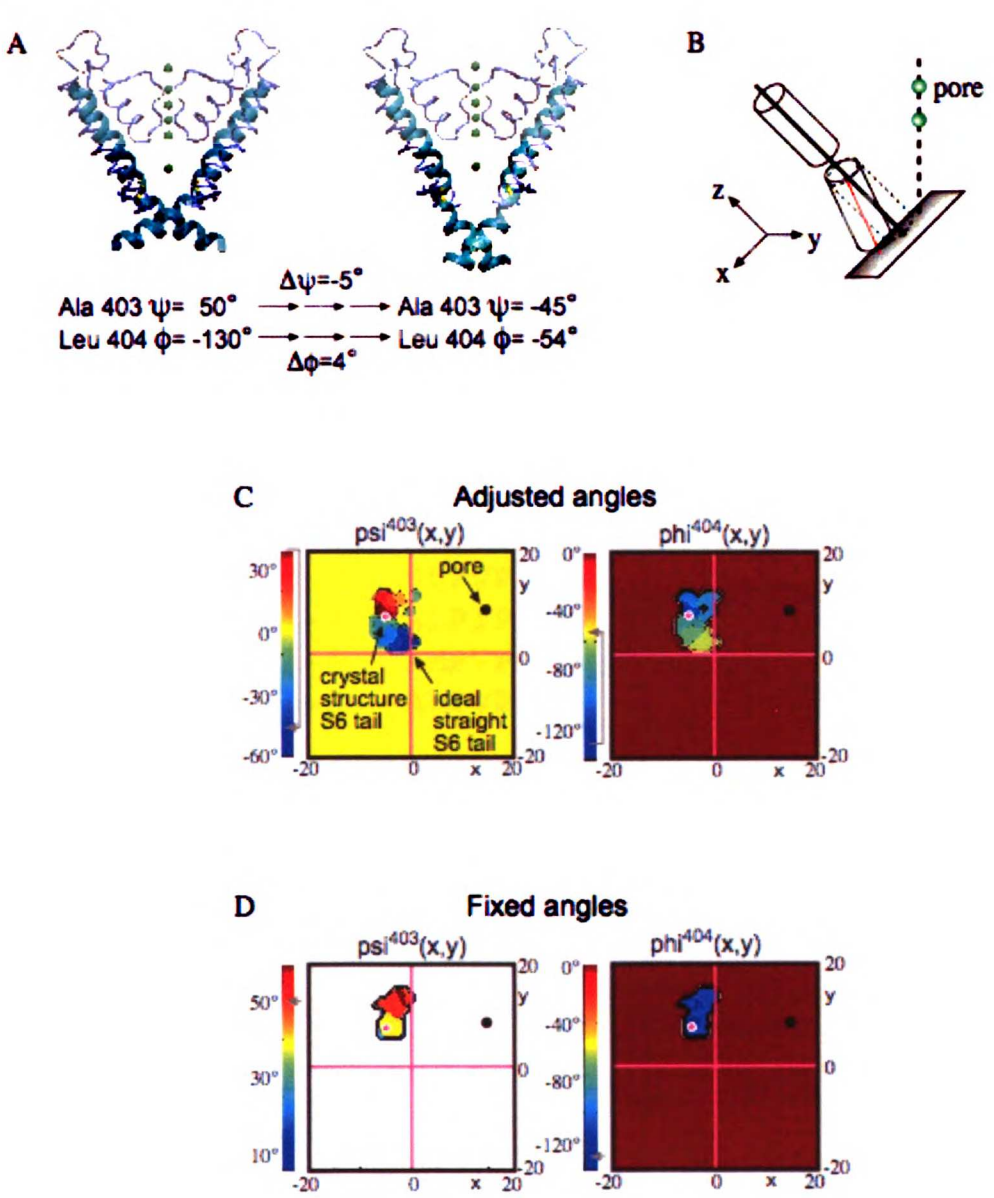

Figure 3: A) Kv1.2 crystal structure and angle-adjusted simulation output superposed on the rest of channel pore, B) inner helix tail tracking diagram. The dashed line indicates the central pore axis of the channel. Two green spheres represent the positions of potassium ions in the selectivity filter, C) and D) $\phi^{404}(x,y)$ and $\psi^{403}(x,y)$ for C) adjusted angles and D) fixed-angle control. The color bar reflects the value of the dihedral angle being monitored (ϕ^{404} or ψ^{403}).

Kv1.1-6	ALPVP
Kv1.7	SLPVP
Kv2.1-2	ALPIP
Kv3.1-4	AMPVP
Kv4.1-3	ALPVP

A/S-L/M-P-V/I-P

Figure 4: Alignment of Kv channels' X-X-P-V/I-P region and resulting motif.

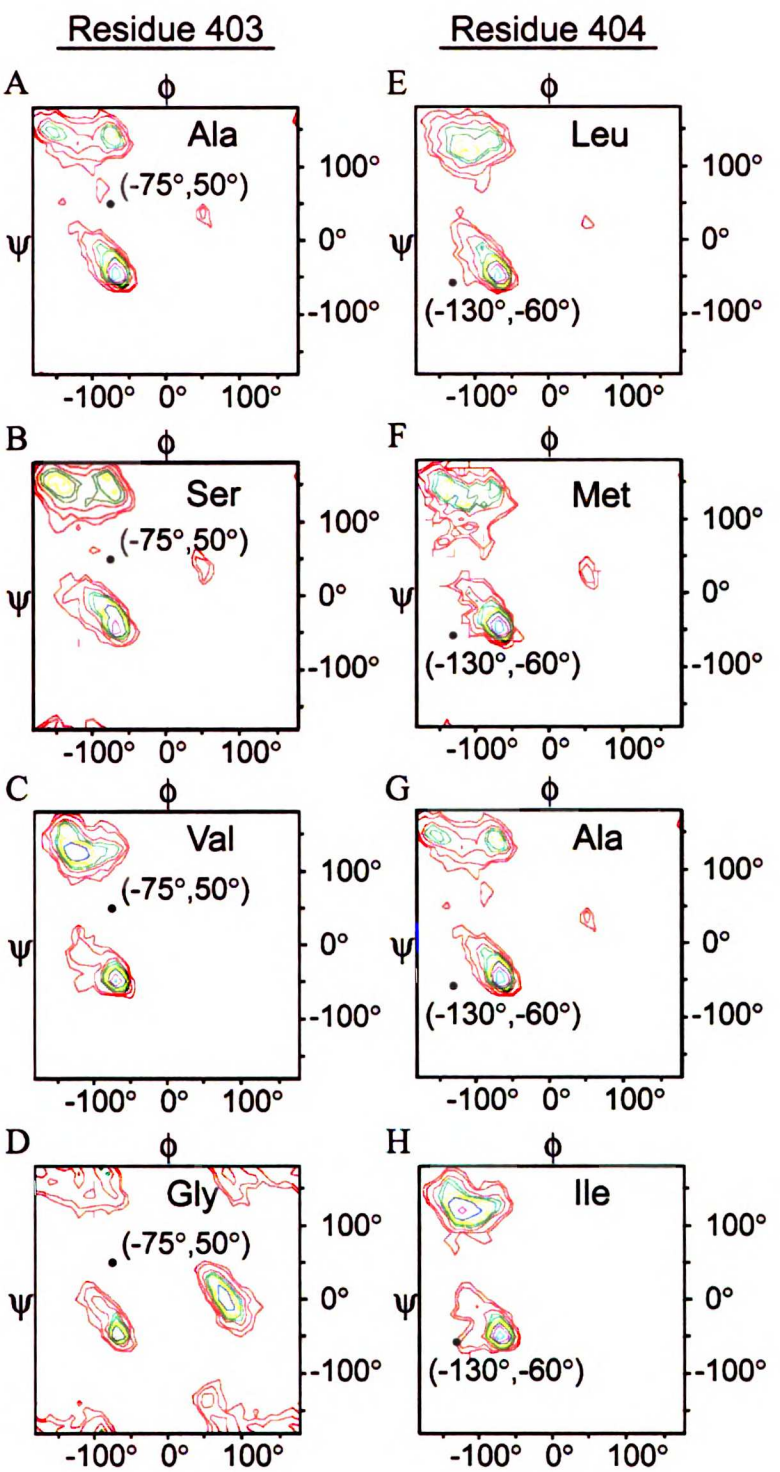

Figure 5: Ramachandran plots of residues of interest for positions 403 (left column) and 404 (right column) (Lovell *et al.*, 2003). The dihedral angle coordinate (ϕ, ψ) of Ala^{403} and Leu^{404} from the Kv1.2 crystal structure is marked in the left column and right column of panels, respectively.

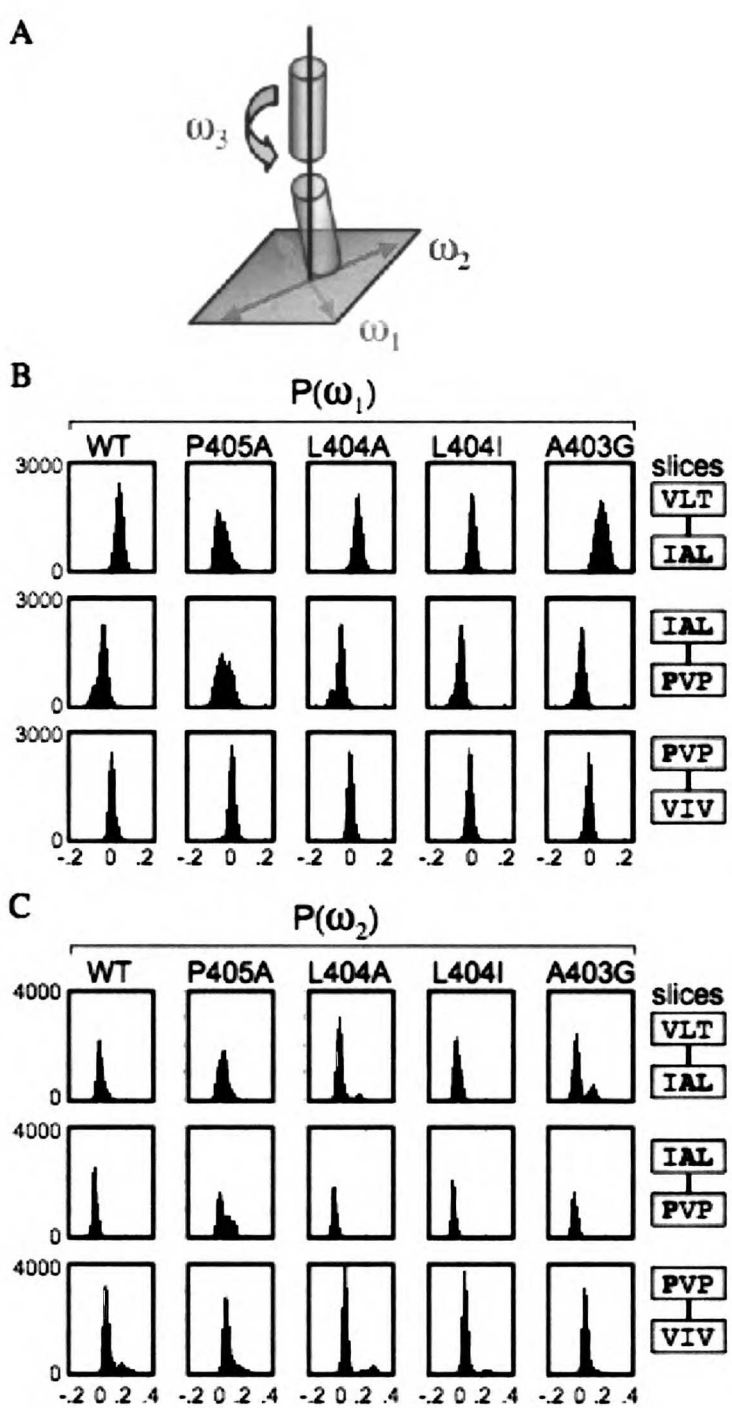

Figure 6: Elasticity and anisotropy of helix bending. A) bending moduli diagram indicating the principal directions in relationship to the helix, B) $P(\omega_1)$ and C) $P(\omega_2)$ distribution (ω_3 data omitted). The y-axis represents the number of observations of the given angle during the course of the simulation. The x-axis is the angle between two successive slices (radians). Histograms were constructed using 100 bins. Residues mutated *in silico* noted in bold.

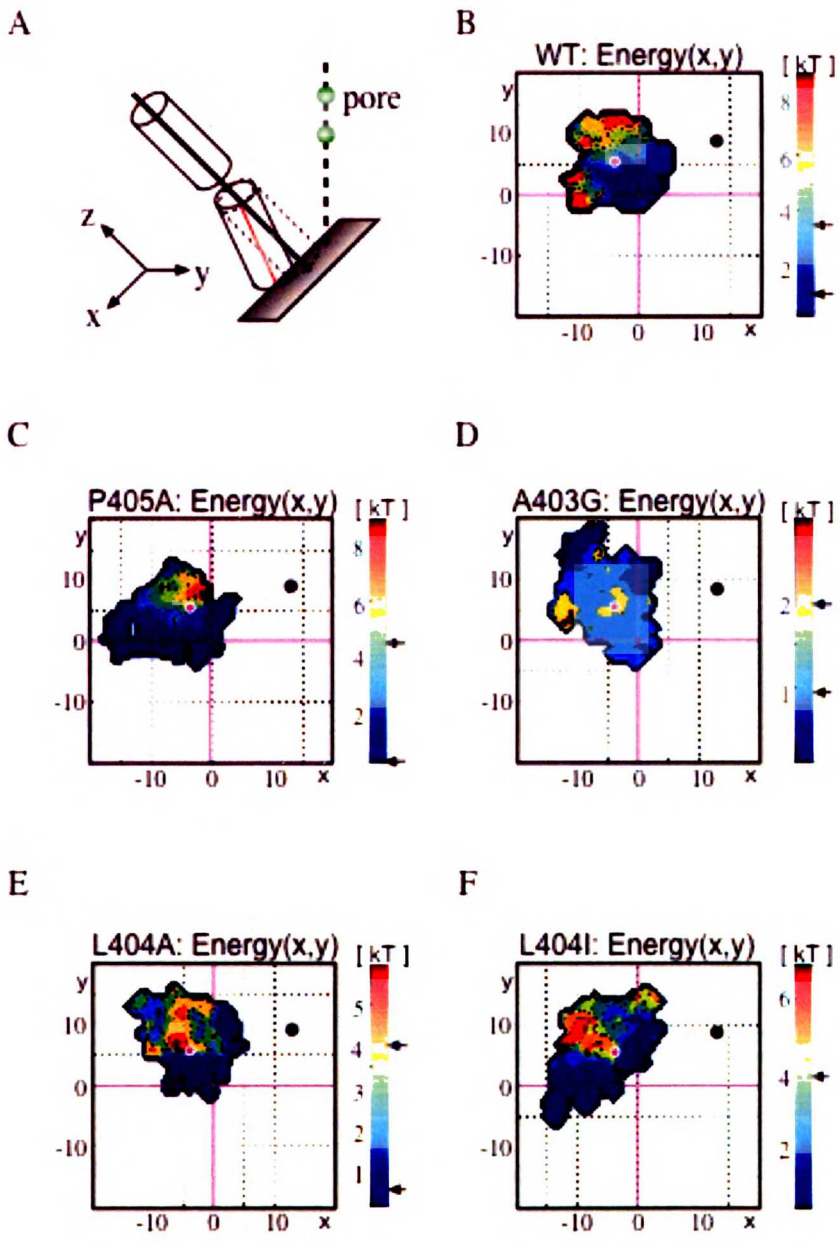

Figure 7: A) Inner helix tail tracking diagram, B)-F) Energy over tail-tracking plane for WT, P405A, A403G, L404A, and L404I. Note different energy scales. Black arrows indicate the energy values near the open and closed configurations.

REFERENCES

Ashcroft, F. M. (2006). From molecule to malady. Nature **440**: 440-7.

Choe, S. and S. X. Sun (2005). The elasticity of α-helices. J Chem Phys **122**: 244912-20.

Chou, P. Y. and G. D. Fasman (1974). Conformational parameters for amino acids in helical, β-sheet, and random coil regions calculated from proteins. Biochem **13**: 211-22.

Clayton, G. M., W. R. Silverman, *et al.* (2004). Structural basis of ligand activation in a cyclic nucleotide regulated potassium channel. Cell **119**: 615-27.

del Camino, D., M. Holmgren, *et al.* (2000). Blocker protection in the pore of a voltage-gated K^+ channel and its structural implications. Nature **403**: 321-5.

Doyle, D. A., J. M. Cabral, *et al.* (1998). The structure of the potassium channel: molecular basis of K^+ conduction and selectivity. Science **280**: 69-77.

Garcia, A. E. and K. Y. Sanbonmatsu (2001). α-Helical stabilization by side chain shielding of backbone hydrogen bonds. Proc Natl Acad Sci USA **99**: 2782-7.

Hackos, D., T. Chang, *et al.* (2002). Scanning the intracellular S6 activation gate in the Shaker K^+ channel. J Gen Physiol **119**: 521-31.

Jiang, Y., A. Lee, *et al.* (2002a). Crystal structure and mechanism of a calcium-gated potassium channel. Nature **417**: 515-22.

Jiang, Y., A. Lee, *et al.* (2002b). The open pore conformation of potassium channels. Nature **417**: 523-6.

Jiang, Y., A. Lee, *et al.* (2003a). X-ray structure of a voltage-dependent K^+ channel. Nature **423**: 33-41.

Jin, T., L. Peng, *et al.* (2002). The βγ subunits of G proteins gate a K^+ channel by pivoted bending of a transmembrane segment. Mol Cell **10**: 469-81.

Karplus, P. A. (1996). Experimentally observed conformation-dependent geometry and hidden strain in proteins. Protein Sci **5**: 1406-20.

Korobi, A., N. Sarai, *et al.* (2003). Additional gene variants reduce effectiveness of beta-blockers in the LQT1 form of Long QT syndrome. J Cardiovasc Electrophysiol **15**: 190-9.

Kumar, S., D. Bouzida, *et al.* (1992). The weighted histogram analysis method for free-energy calculations on biomolecules. I. The method. J Comp Chem **13**:1011-21.

Kumar *et al.* (1995). Multidimensional free-energy calculations using the weighted histogram analysis method. J Comp Chem **16**: 1339-50.

Labro, A. J., A. L. Raes, *et al.* (2003). Gating of *Shaker*-type channels requires the flexibility of S6. J Biol Chem **278**: 50724-31.

Lehmann-Horn, F. and K. Jurkat-Rott (1999). Voltage-gated ion channels and hereditary disease. Physiol Rev **79**: 1317-72.

Long, S. B., E. B. Campbell, *et al.* (2005). Crystal structure of a mammalian voltage-dependent *Shaker* family K^+ channel. Science **309**: 897-903.

Lovell, S., I. W. Davis, *et al.* (2003). Structure validation by Cα geometry: ϕ, ψ, and Cβ deviation. PROTEINS: Struct, Funct, and Genet **50**: 437-50.

Magidovich, E. and O. Yifrach (2004). Conserved gating hinge in ligand- and voltage-dependent K^+ channels. Biochem **43**: 13242-7.

Minor, D. L., S. J. Masseling, *et al.* (1999). Transmembrane structure of an inwardly rectifying potassium channel. Cell **96**: 879-91.

Perozo, E., D. M. Cortes, *et al.* (1999). Structural rearrangements underlying K^+-channel activation gating. Science **285**:73-8.

Ri, Y., J. A. Ballesteros, *et al.* (1999). The role of a conserved proline residue in mediating confromational changes associated with voltage gating of Cx32 gap junctions. Biophys J **76**: 2887-98.

Seebohm, G., N. Strutz-Seebohm, *et al.* (2006). Differential roles of S6 domain hinges in the gating of KCNQ potassium channels. Biophys J **90**: 2235-44.

Webster, S., D. del Camino, *et al.* (2004). Intracellular gate opening in Shaker K^+ channels defined by high-affinity metal bridges. Nature **428**: 864-8.

Yifrach, O. and R. MacKinnon (2002). Energetics of pore opening in a voltage-gated K^+ channel. Cell **111**: 231-9.

For reference

Not to be taken from the room.